

# Automatic Segmentation of Colonic Polyps in CT Colonography Based on Knowledge-Guided Deformable Models

Jianhua Yao, Meghan Miller, Marek Franaszek, Ronald M. Summers

Diagnostic Radiology Department, Clinical Center, NIH

## ABSTRACT

An automatic method to segment colonic polyps from CT colonography is presented. The method is based on a combination of knowledge-guided intensity adjustment, fuzzy c-mean clustering, and deformable models. The input is a set of polyp seed points generated by filters on geometric properties of the colon surface. First, the potential polyp region is enhanced by a knowledge-guided adjustment. Then, a fuzzy c-mean clustering is applied on a 64\*64 pixel sub-image around the seed. Fuzzy membership functions for lumen air, polyp tissues and other tissues are computed for each pixel. Finally, the gradient of the fuzzy membership function is used as the image force to drive a deformable model to the polyp boundary. The segmentation process is first executed on the 2D transverse slice where the polyp seed is located, and then is propagated to neighboring slices to construct a 3D representation of the polyp. Manual segmentation is performed on the same polyps and treated as the ground truth. The automatically generated segmentation is compared with the ground truth segmentation to validate the accuracy of the method. Experimental results showed that the average overlap between the automatic segmentation and manual segmentation is 76.3%. Given the complex polyp boundaries and the small size of the polyp, this is a good result both visually and quantitatively.

**Keywords:** Colonic polyp segmentation, fuzzy c-mean cluster, deformable model

## 1. BACKGROUND AND INTRODUCTION

CT colonography has been used for detection and screening of colonic cancers. The purpose of the test is to locate and identify the polyps on the colon wall. Several systems are under development to bring Computer Aided Detection of colonic polyps into clinical use. Most of them use geometric features on colon surfaces and/or volumetric properties near the surface to assist the detection. While current results seem promising, there are some arguments that better features need to be computed for better classification. Polyp segmentation is imminent since it will provide the entire voxel set of the polyp, which can be used to quantify the characteristics of the polyp. Several comprehensive volumetric features and statistical analysis can be obtained, such as the density, the volume and dimension of the polyp, and its relationship with surrounding tissues. Polyp segmentation can also be directly applied in the detection of polyps. If the segmentation process fails at a polyp candidate, it may indicate that the detection is a false positive. Once the segmentation is obtained, additional analysis such as texture analysis can be performed. We define the segmentation of a polyp to be a surface that encloses the polyp and its interior voxels. On a 2D transverse slice, it is a closed polygon (contour) representing the boundary of the polyp.

Colonic polyp segmentation is a complex task for several reasons. First, polyp shapes are irregular. Second, the sizes of polyps vary greatly. Third, the surrounding regions are complex. Figure 1 shows some typical polyp examples in CT colonography. Figure 1(a) shows a classic medium size round shape polyp protruding to the colon lumen. This type of polyp is relatively easy to segment by analyzing edgels in the image and the shape of polyps. Figure 1(b) is a tiny polyp only a few pixels in size, and Figure 1(c) is a flat polyp. Figure 1(b) and 1(c) are easy to miss during CT colonographic exams. Figure 1(d) is a polyp on a fold, and Figure 1(e) is a polyp connecting to a fold. It should be noted that sometimes the shape of a fold is very similar to that of a polyp in CT colonography. Figure 1(f) and 1(h) are big masses, which tend to have irregular shape and occupy most of the local colon segment and may be difficult to get

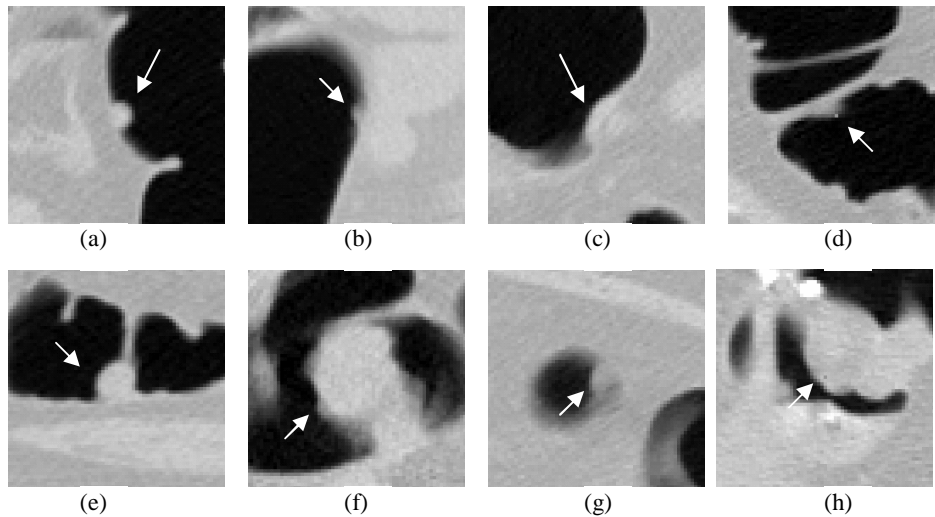


**Figure 1. Polyp examples in CT colonography**  
 (a) Perfect medium round polyp; (b) Tiny polyps; (c) Flat polyps; (d) Polyp on fold; (e) Polyp connected to a fold; (f) Big Mass; (g) Blurry boundary; (h) Complex scene

complete regions just based on geometric features. In Figure 1(g) and 1(h), the polyp is in a very complex surrounding region, and no obvious boundary can be identified. A single shape or densitometry template is not sufficient to describe all polyps in Figure 1. A more sophisticated method utilizing both the shape and densitometry information is necessary for successful colonic polyp segmentations. The boundary between the polyp and the lumen is relatively easy to locate due to the large intensity discrepancy between these two regions. But the boundaries between polyp tissues and non-polyp tissues are not very obvious. Sometimes the polyps are connected to other objects in the images, such as in Figure 1(e), 1(f) and 1(h). Special image processing procedures need to be applied in order to successfully locate and separate them.

There are several existing methods for colonic polyp segmentation. Yoshida and Nappi et al [1, 2] proposed a polyp segmentation method by means of hysteresis thresholding with use of some volumetric features. They first located the voxels with low curvedness values and high shape index (cup shape) and then clustered them to segment the polyp. Their method doesn't work well for small polyps and flat polyps since there is an insufficient number of voxels with low curvedness values and high shape index for clustering. Their method may also have trouble in segmenting big masses where the shape of polyps are usually irregular and voxels in the polyp region may not have similar curvedness and shape index to be clustered together. Jerebko *et al.* [3] used Radon transformation and Canny edge to detect polyp boundaries. They first used Canny edge detectors to locate the polyp-lumen boundary, and used Radon transformation to identify round shape polyps. In the existing literature, no segmentation algorithm has been reported to robustly segment all types of polyps listed in Figure 1. The goal of our investigation is to develop an automatic and robust method that can accurately segment most existing polyps which can be manually segmented by an expert. We are not tackling those polyps that can not even be segmented by a human.

The rest of the paper is organized as follows. Section 2 introduces our method. Section 3 presents our experimental data and results. Finally, Section 4 provides some discussions and future plans.

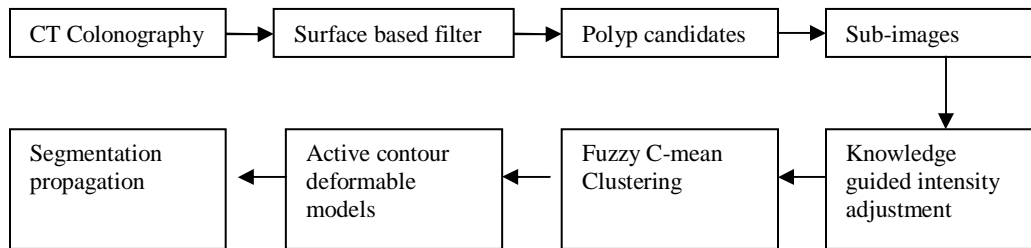


**Figure 2 Colonic segmentation flow chart**

## 2. METHODS

Our approach is a combination of fuzzy clustering and deformable models. The method is also guided by prior knowledge about the colonic polyp. Both intensity distribution and shape properties are utilized. Our method is illustrated in Figure 2. First CT colonography is performed on high risk patients undergoing colon cancer screening. The colon surface is extracted using an existing software package. [4, 5] For each point on the surface, geometric and local volumetric properties are analyzed and filtered to get a set of polyp candidate seeds. The candidate pool is usually a large set, including true positive and false positive detections. Multiple detections may occur on a single polyp. The segmentation algorithm takes the candidate seed as the input. Ideally, at the location of true positive detections, an accurate segmentation should be obtained, whereas at the location of false positive detections, no segmentation should be found. From our observation, polyp detection is a local operation, i.e. only a local region around the polyp need be examined to identify the polyp. Therefore, a 64\*64 pixel sub-image centered at the candidate seed is first obtained. All following operations are conducted on the sub-image to reduce the computational time and artifacts from un-related tissues. First, a knowledge-guided intensity adjustment procedure is conducted to enhance potential polyp regions. Then, a fuzzy c-mean clustering is applied to compute the membership values of lumen, polyp tissue and non-polyp tissue for each voxel in the sub-image. From the clustering, we can roughly classify every pixel in the image and get the approximate region of the polyp. An initial deformable model is placed in the centroid of the initial region of polyp. The deformable model is then driven by the image force computed from the membership map of polyp tissues, together with an external balloon force and the intrinsic model force. After several iterations, the deformable model converges to the potential polyp boundary. Once the segmentation (a closed contour) is generated on one slice, the procedure is propagated to neighboring slices. The process is iterated until no segmentation can be found or the segmentations on adjacent slices are not continuous (the overlap is too small). At the end, all 2D segmentations are stacked up to build a 3D segmentation.

The details of our approach, especially the knowledge guided intensity enhancement, the fuzzy clustering, and the deformable model technique will be elaborated in following subsections.

### 2.1 Knowledge guided intensity adjustment

Given a CT colonography, sometimes it is difficult to differentiate polyp tissues and non-polyp tissues based on their CT numbers (image intensity) (see figure 3a). However, assisted by knowledge of surrounding regions and shape of polyps, an expert is able to identify the polyp. Colonic polyps usually appear as protrusions from the colon wall into the lumen air. This knowledge can be used to assist the polyp segmentation.

We designed a knowledge guided intensity adjustment method to enhance the potential polyp region in CT colonography. Two pieces of knowledge have been used in our method:

- 1) the polyp abuts the lumen air

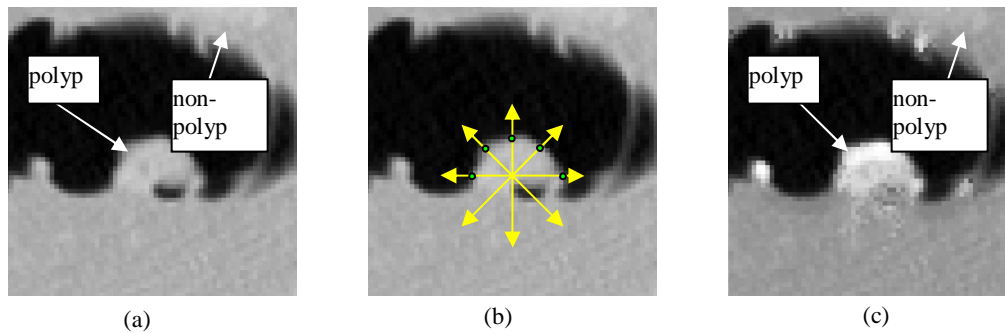


**Figure 3 Knowledge guided intensity adjustment**

(a) original image; (b) scoring of a pixel, arrows are the shooting directions, circles are hit points; (c) enhanced image

2) the polyp-lumen boundary tends to have convex curvature

In our method, first the iso-boundary between the lumen air and the colon wall is located. Since the lumen air has HU number around -1000 and the soft tissue has HU number larger than -500, the iso-boundary can be accurately locating using an iso-value of -700. The volumetric curvatures of the iso-boundary are computed using equation 1.

$$\kappa = \frac{f_{xx}f_y^2 - 2f_xf_yf_{xy} + f_{yy}f_x^2}{(f_x^2 + f_y^2)^{3/2}} \quad (1)$$

where  $\kappa$  is the volumetric curvature,  $f_x, f_y$  are first derivatives of the image intensity,  $f_{xx}, f_{xy}, f_{yy}$  are second derivatives of the image intensity. Then the boundaries are categorized into three classes according to their curvatures: convex, flat, and concave. A threshold value of curvature ( $C_{th}$ ) is supplied to classify different types of boundaries. The boundaries with curvature greater than  $C_{th}$  are concave boundaries, those with curvature smaller than  $-C_{th}$  are convex boundaries, and the rest are flat boundaries.  $C_{th}$  in our experiment is  $0.15 \text{ pixel}^{-1}$ .

Each pixel in the image is then given a score based on its relative location to the iso-boundaries. To assign the score to a pixel  $v$ , a set of evenly spaced rays are shot from  $v$  in different directions  $d_k$  (see figure 3(b)). If the rays hit the iso-boundary within a distance, some scores will be added to pixel  $v$ . The score of pixel  $v$  is given as

$$score(v) = \sum_{k=1}^{Nd} E(d_k(v), s) \quad (2)$$

$$E(d_k(v), s) = \begin{cases} 2, & \text{hit a convex boundary within distances} \\ 1, & \text{hit a flat boundary within distances} \\ 0, & \text{hit a concave boundary within distances} \\ -1, & \text{no hit within distances} \end{cases}$$

here the number of ray directions ( $Nd$ ) used in our method is 24 (15 degree apart), and the distance  $s$  is the maximum diameter of a polyp (30 mm in our method). Under this scoring scheme, the pixel will be awarded a high score if it is next to convex boundaries, and will be penalized if it is not. The intensity of a pixel is then adjusted based on its score as follows:

$$Adjustment(v) = \begin{cases} 100HU, & \text{if } score(v) > Nd/2 \\ 50HU, & \text{if } Nd/2 \geq score(v) \geq Nd/4 \\ 0HU, & \text{if } Nd/4 > score(v) \geq 0 \\ -50HU, & \text{if } score(v) < 0 \end{cases} \quad (3)$$

The intensity of pixel is increased if it is in a potential polyp region; otherwise, the intensity is decreased.

Figure 3 shows the knowledge-guided intensity adjustment. Figure 3(a) is the original image, where polyp regions and non-polyp tissue region have very similar intensity values. Figure 3(b) is the illustration of shooting rays from a pixel to compute its score. Figure 3(c) is the enhanced image after the intensity adjustment. All following operations are performed on the enhanced image.

## 2.2 Fuzzy C-mean clustering

Fuzzy segmentation has been favored over hard segmentation in some medical image applications. In CT colonography, the shapes of colonic polyps are irregular and varied, and the surrounding regions are complex. There are partial volume effects due to the large slice spacing and image noise in soft tissues. Moreover, it is difficult to determine a threshold to differentiate the polyp regions and the non-polyp regions. We apply a fuzzy c-mean (FCM) clustering method to first classify pixels in the image into several tissue categories.

FCM is a popular clustering technique used in non-supervised image segmentation for pixel classification and pattern recognition purposes. [6] In FCM methods, a set of tissue classes is first determined. Then each voxel is classified by computing its membership functions of the tissue classes according to its intensity. The value of membership functions is restricted to the range 0 to 1. The sum of all membership values over all classes for any voxel is 1. The value of the membership function of one class indicates the likelihood of the pixel belonging to that class. Each tissue class has a centroid. The objective of FCM clustering is to find the membership functions for each pixel so that they are clustered around the centroid of each class. FCM can be written as the minimization of the following objective function:

$$F = \sum_{x \in \Omega} \sum_{k=1}^N u_k(x)^2 \|y(x) - c_k\|^2 \quad (4)$$

here,  $\Omega$  is the set of pixels in the image,  $N$  is the total number of tissue classes,  $u_k(x)$  is the membership function value of pixel  $x$  for class  $k$  subject to  $\sum_{k=1}^N u_k(x) = 1$ ,  $y(x)$  is the observed image intensity of pixel  $x$ , and  $c_k$  is the centroid of class  $k$ . The objective function is minimized when a large membership value of a class is assigned to a pixel when it is close to the centroid of that class. This is a non-linear problem and can be solved iteratively. During each iteration, a new set of membership functions and class centroids are computed. The following steps describe the FCM algorithm.

1. provide the initial values for class centroids,  $c_k, k=1..N$
2. compute the membership functions

$$u_k(x) = \frac{\|y(x) - c_k\|^{-2}}{\sum_{l=1}^N \|y(x) - c_l\|^{-2}} \quad (5)$$

3. compute the new centroid for each class

$$c_k = \frac{\sum_x u_k^2(x) y(x)}{\sum_x u_k^2(x)} \quad (6)$$

4. repeat step 2 and step 3 until the algorithm converges. Convergence is reached when the maximum change in the membership functions over all pixels between two iterations is less than a predefined small value.

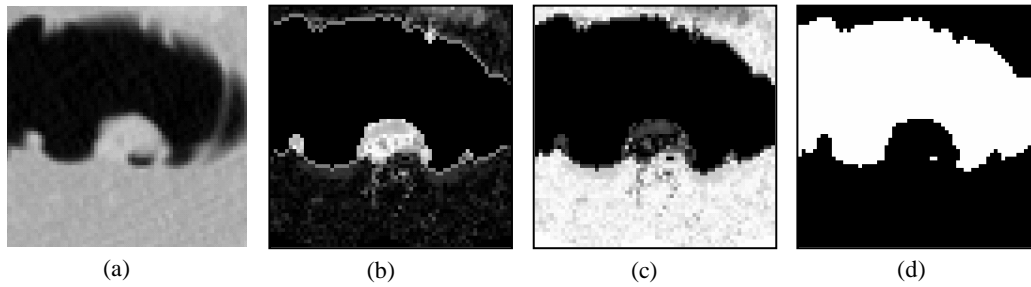


**Figure 4 Fuzzy clustering results**

(a) original image; (b) polyp tissue membership map; (c) non-polyp tissue membership map; (d) lumen air membership map

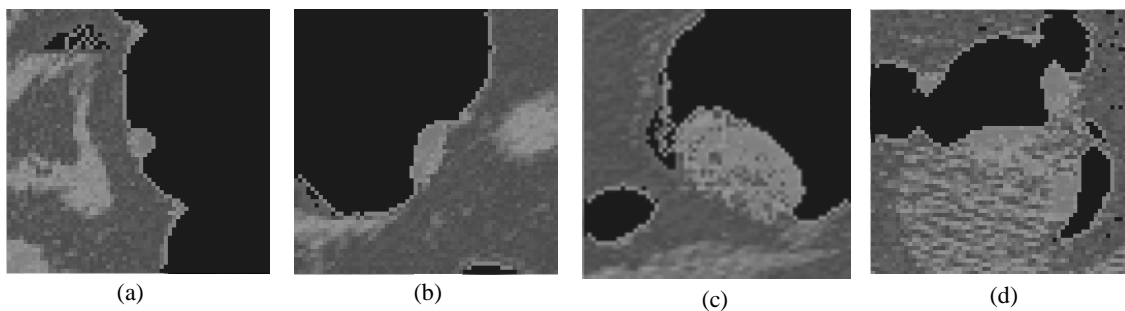


**Figure 5 More fuzzy clustering results**

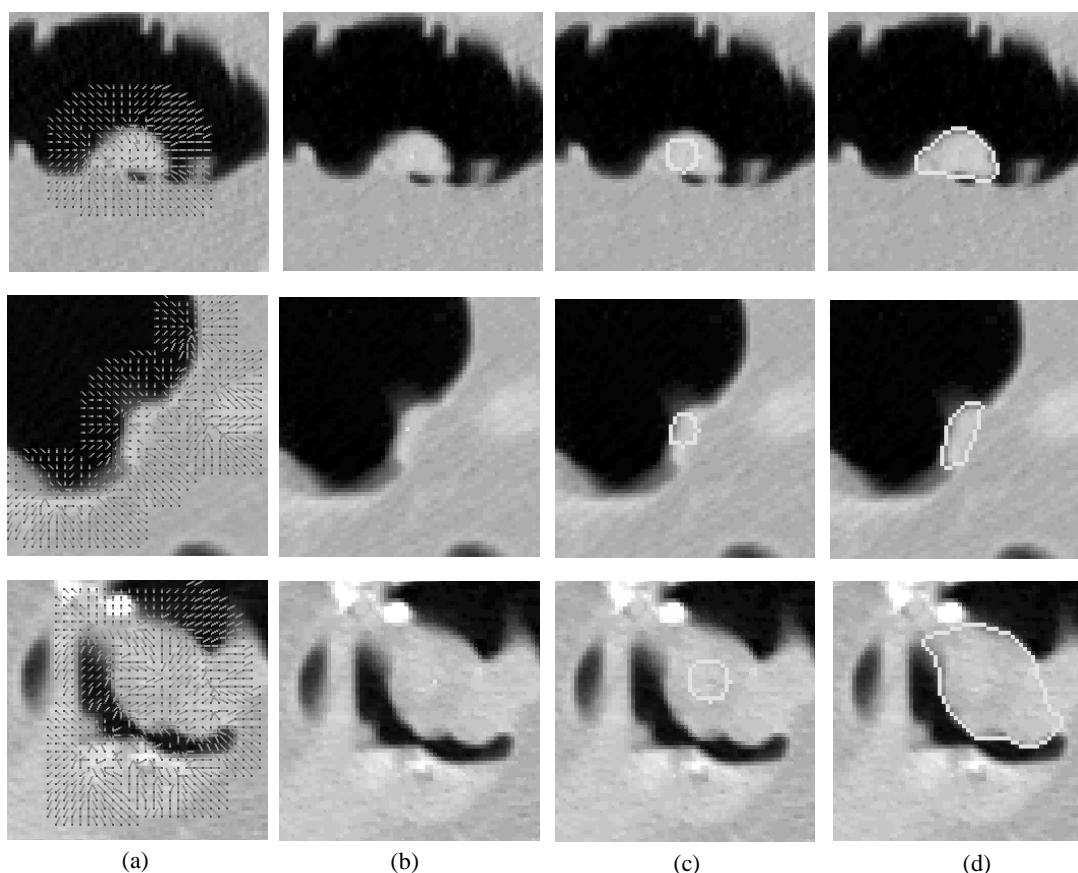
We have defined three tissue classes in the polyp segmentation: lumen air, polyp tissues and non-polyp tissues. Three membership values are computed for each pixel. The initial estimate of each class centroid is derived from a priori knowledge about the intensity distribution and the seed position. The initial centroid for lumen air is a small value (e.g.  $-900$  HU). The centroid of polyp tissues is given as the average intensity of the enhanced region in a neighborhood of the seed location, and that of non-polyp tissues is the average intensity of the non-enhanced region in the same neighborhood. The neighborhood used in our method is a  $15\text{mm}$  circle around the seed.

Figure 4 shows some results of the fuzzy clustering. Figure 4a is the sub-image around a seed point. Figure 4 (b-d) shows the membership map for lumen air, polyp tissues and non-polyp tissues respectively. Brighter color in the map indicates higher membership value. Figure 5 are more examples of fuzzy clustering in various polyp shapes and surrounding regions. We use different color channels to represent different membership functions. Lumen air is represented in blue channel, non-polyp tissues in red channel, and polyp tissues in green channel. From the fuzzy clustering, we can approximately identify the polyp region. But there is still a lot of noise, and the boundaries between polyp tissues and non-polyp tissues are blurry. In the cases in Figure 4 and Figure 5(a-b), the fuzzy clustering provides very clear polyp regions. But in Figure 5(c) and 5(d), the region is very noisy, further processing is necessary.

### 2.3 Deformable model

The result of the fuzzy clustering can be converted to a hard segmentation by assigning each pixel to the class with highest membership value. But due to the noise and complexity in the scene, the result may not be a good segmentation. Furthermore, colonic polyps have irregular shapes and threshold-based segmentation usually results in discontinuous and unsmooth regions. Therefore, we developed a method to use the membership function as the force to drive a deformable model to obtain the polyp segmentation.

Deformable models have been widely used in medical image segmentation. The active contour model is the most commonly used deformable model in 2D image segmentation. The active contour model was first introduced by Kass and Terzopoulos *et al.* [7] Several researchers improved this method by adding features for different applications.



**Figure 6 Result of deformable models**  
 (a) image force map; (b) initial model; (c) after 5 iterations; (d) final results

Cohen *et al.* [8] proposed a balloon force that significantly increases the capture range. The advantage of using active contour is that it ensures the smoothness and continuity of the boundary. The final representation of the contour is obtained based on different forces being used.

Given an initial contour, several forces work together to drive the active contour to its destination. The forces that drive the active contour model can be expressed as:

$$F = w_{in}F_{internal} + w_{im}F_{image} + w_{ex}F_{external} \quad (7)$$

where  $F_{internal}$  is the spline force of the contour,  $F_{image}$  is the image force, and  $F_{external}$  is the external force, and  $w_{in}$ ,  $w_{im}$  and  $w_{ex}$  are the respective weighting parameters. The internal force  $F_{internal}$  can be written as:

$$F_{internal} = \frac{1}{2} \int_0^1 (\alpha(s)|x'(s)|^2 + \beta(s)|x''(s)|^2) ds \quad (8)$$

where  $x(s)$  is the curve representing the contour,  $x'(s)$  is the first order derivative of  $x(s)$ , and  $x''(s)$  is the second order derivative of  $x(s)$ . The spline force is composed of a first-order term controlled by  $\alpha(s)$  and a second-order term controlled by  $\beta(s)$ . The first-order term makes the contour act like an elastic membrane, and the second-order term makes it act like a thin rigid plate. By adjusting the weights  $\alpha(s)$  and  $\beta(s)$ , one can control the relative importance of the membrane term and the thin-plate term.  $\alpha(s)$  and  $\beta(s)$  may be different at different values of  $s$  and at different iterations. In our implementation, we keep  $\alpha(s)$  and  $\beta(s)$  constant for every  $s$  throughout the procedure, and  $\alpha(s) = 0.5$  and  $\beta(s) = 1$ .

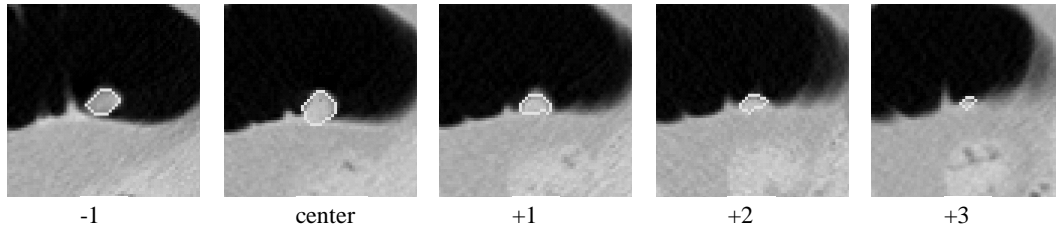


**Figure 7 Segmentation propagation**

The internal force is used to guarantee the smoothness and continuity of the contour, and to prevent the contour moving freely or bending too much.

$F_{image}$  are forces derived from the image to attract the contour to image features such as edges, iso-values, or boundaries. In our method, we use the gradient of the membership function as the image force to attract the deformable contours to the polyp boundary, i.e.

$$F_{image} = Max_{\phi}(\bar{g}) \quad (9)$$

where  $\bar{g}$  is the gradient on membership function map,  $Max_{\phi}(\ )$  is a maximum filter over a 5\*5 template region. The maximum filter is similar to a median filter instead a maximum value is preserved. The maximum filter is applied to the gradient map to increase the capture range and reduce the noise. .

$F_{external}$  are forces added by users for different applications. Similar to the balloon forces proposed by Cohen et al., [8] we added an external force to push the contour away from the centroid. The external balloon force at a vertex  $v_x$  can be written as

$$F_{balloon} = \frac{v_x - v_c}{\|v_x - v_c\|} \quad (10)$$

where  $v_c$  is the centroid of the current contour. The active contour converges when all forces reach a balance. Active contour models need an initial value close to the objective model.

We apply the active contour model using the polyp tissue membership map. The initial contour is a half-pixel radius circle placed at the centroid of all pixels within a range of the seed point with polyp tissue membership values greater than 0.5. The weights for different forces are  $w_{in}=1$ ,  $w_{im}=1$ , and  $w_{ex}=1$ , respectively.

Figure 6 shows some results. Figure 6a shows the image force generated by the gradient of the membership map. Figure 6b shows the initial contour. Figure 6c shows the intermediate state of the contour after 5 iterations, and figure 6d shows the final result. We can see that the deformable model converges to the polyp boundaries under the guidance of image and balloon forces. The internal forces keep the contour smooth and continuous. The interior regions of the polyp boundaries are filled and used as the representation for polyp segmentation.

## 2.4 Segmentation propagation

Colonic polyps are 3D objects. The technique presented in this paper is based on one 2D transverse slice. We designed a scheme to propagate the segmentation to 3D space. First the segmentation is computed on the slice where the seed point is located. Then the segmentation is propagated to adjacent slices (next slice and previous slice) using the centroid of the current segmentation as the seed point. The propagation stops when no segmentation can be found or the segmentations between two adjacent slices are not continuous, i.e., the overlap between two segmentations is smaller than a given value. Figure 7 shows the 3D segmentation of a polyp. It covers 5 transverse slices. Slice 2 is the location of

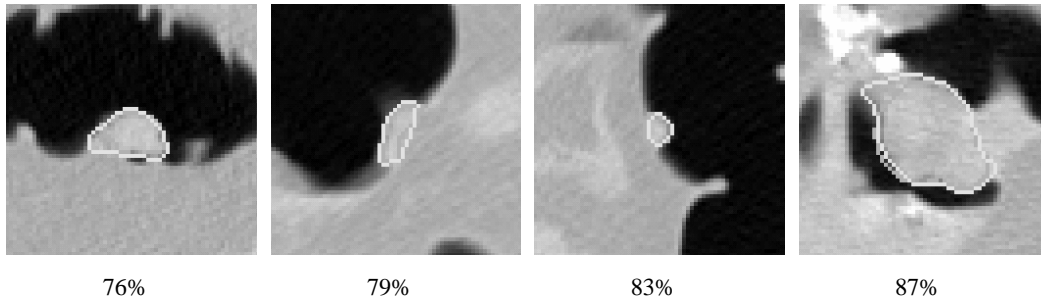


**Figure 8 Comparison of manual painting and automatic segmentation**

the seed point (center slice). Our technique is essentially a 2D technique. A true 3D technique using deformable surface is under development.

### 3. EXPERIMENTS AND RESULTS

The CT colonography data used in our experiment were obtained from 20 patients (each patient had a supine study and a prone study). CT scans were done on a GE Hispeed scanner. The scanning parameters were 120 KVp, 50 mAs (mean), field of view to fit (38-46 cm), 5 mm collimation, HQ mode, and 3 mm reconstruction interval. The data size was  $512 \times 512 \times N$ , where  $N$  is the number of transverse slices, which is around 300. Based on colonoscopic examination and CT colonography of the same patient, 65 polyps were identified.

First, We extracted the colon surface from the CT colonography. We then applied a filter to every vertex on the surface based on its geometric and volumetric attributes. The output of the filter is a set of seed points. Among the seed points, some are true positive detections, some are false positive detections. The filter on our data set generated 105 true positive detections (with multiple detections of the same polyp). For each true positive detection, we applied the automatic segmentation method to obtain the polyp boundaries. The segmentation method was robust enough to segment all true positive detections. The results in figure 6-8 show that the segmentation visually matches the polyp boundary. In order to quantitatively validate the accuracy of our segmentation method, we manually painted all true positive detections and stored the painting in a database. The polyp painting was carefully performed by a trained student and verified by an experienced radiologist. The manual painting was used as the ground-truth segmentation in our study. Figure 8 shows several manual paintings together with automatic segmentation. The blue (dark) contours are the manual painting and the yellow (bright) contours are the automatic segmentations. We validate the accuracy of the automatic segmentation results by computing the overlap between the manual painting and the automatic segmentation. The overlap is computed as

$$overlap = \frac{2\|c_s \cap c_p\|}{\|c_s\| + \|c_p\|} \times 100\% \quad (11)$$

here  $c_s$  is the automatic segmentation, and  $c_p$  is the manual painting,  $\|\bullet\|$  represent the number of voxels in a segmentation. Among all 105 true positive detections, the average overlap was 76.3%, the standard deviation was 21.7%, the minimum overlap was 34.4%, and the maximum overlap was 95.5%. From the observation in Figure 8, we notice that 80% overlap is relatively good considering the small size of the colonic polyps.

#### 4. DISCUSSIONS AND FUTURE WORKS

We have developed an automatic colonic polyp segmentation method for CT colonography. The technique combines knowledge guided intensity adjustment, fuzzy c-mean clustering, and deformable models. It uses both intensity properties and geometric properties of the polyp.

We validated the automatic segmentation by comparing the automatic segmentation results with manual painting. This is the first use of such method in colonic polyp segmentation. The results show that the automatic segmentation matches well the manual segmentation. In some cases, the automatic segmentation is better since it is more consistent and smoother. The manual painting database can not only serve as the ground truth segmentation, it can also be used to separate true positives and false positives in the training phase. Furthermore, it can be used directly in the training to extract the common properties of true positive detections of colonic polyps.

Colonic polyp segmentation is not an easy task due to the irregular shape of colonic polyps and the complex surrounding regions. We first enhance the potential polyp region using a knowledge-guided intensity adjustment process. The adjustment uses the knowledge of the shape of a polyp and its surrounding region. It is possible to use edge detection or texture analysis to locate the potential polyp region, but those methods usually are not robust enough to identify all kinds of polyps. Fuzzy clustering is used to group polyp pixels. An alternative method is to apply threshold techniques to distinguish polyp pixels after the intensity adjustment process. However, it is difficult to obtain a uniform threshold value that differentiates polyp and non-polyp tissues. Furthermore, the threshold technique is usually sensitive to image noise. Fuzzy clustering gives us the probability of one pixel belonging to polyp regions, and can also be used as an image force to drive a deformable model. A region growing plus mathematical morphology on the fuzzy membership map may also provide the polyp segmentation, but it cannot ensure a continuous and smooth boundary. Instead, deformable active contour models driven by fuzzy membership functions provide a consistent and smooth segmentation. The technique is applied on a 64\*64 pixel sub-image around the seed point based on the observation that polyp detection is a local operation. This practice also speeds up the segmentation process and makes the fuzzy clustering less sensitive to other regions in the image. Currently, the segmentation takes less than 1 second to complete on a 1.8GHz Pentium IV PC, and there is still room to further optimize the algorithm.

There are a few things to improve in our colonic polyp segmentation technique. Although the segmentation is propagated to neighboring slices to generate a 3D segmentation, the technique itself is basically 2D and currently no continuity and smoothness constraints are imposed between slices. 3D techniques should be explored to get better segmentation. The 3D techniques would include a 3D fuzzy clustering and a 3D deformable surface model, which are easy to extend from current 2D techniques. 3D techniques require thin between-plane slice thickness to obtain consistent results. The data sets we are working with have 3mm or 5mm reconstruction interval, which is not thin enough for a successful 3D segmentation. We can either do an inter-slice interpolation or turn to more advanced imaging protocols to get thinner slice data.

The segmentation process can also be employed to directly assist polyp detection. Some polyp candidates are true positive detections, but most of them are false positive detections. The segmentation may fail at some seed points under some criteria, e.g., the aspect ratio is too big (usually fold detections), or the average intensity is too big (usually contrast-enhanced stools). Ideally, the segmentation should succeed at all true positive detections (100% sensitivity), and fail at all false positive detections (100% specificity). Since some false positive detections are very similar to true positive detection in CT colonography, it is very difficult to get 100% sensitivity and 100% specificity. But hopefully the segmentation process can retain all true positive detections (100% sensitivity), and at the same time eliminate a portion of false position detections. Since the entire polyp region is available after the segmentation, new volumetric and geometric features can be computed. These features can then be fed to Neural Network (NN) or Support Vector Machine (SVM) for further analysis and classification. Therefore, the segmentation process can improve the polyp detection in two ways: 1) provide a 'cleaner' training set by reducing the number of false positives; 2) provide new features for classification.

We must mention that the quality of the data set we are working on is not very good. The slice interval is big (3mm-5mm). Some colons are not inflated very well. And some colons are not very clean (stools exist). But our segmentation technique is robust enough to segment all the polyps in the data set. We are currently working on a much bigger data set to further test our segmentation technique.

## ACKNOWLEDGMENTS

We thank Andrew Dwyer, MD, for critical reviews of the manuscript. We also thank C. Daniel Johnson, MD of the Mayo Clinic for providing CT colonography data sets.

## REFERENCES

1. Nappi, J. and H. Yoshida, *Automated Detection of Polyps with CT Colonography: Evaluation of Volumetric Features for Reduction of False-Positive Findings*. Academic Radiology, 2002 **9**(4): p. 386-397.
2. Yoshida, H., et al., *Computerized detection of colonic polyps at CT colonography on the basis of volumetric features: pilot study*. Radiology, 2002, **222**(2): p. 327-36.
3. Jerebko, A., M. Franaszek, and R. Summers. *Radon transform based polyp segmentation method for CT colonography computer aided diagnosis*. RSNA. 2002.
4. Summers, R.M., et al., *Automated polyp detection at CT colonography: feasibility assessment in a human population*. Radiology, 2001, **219**(1): p. 51-59.
5. Summers, R.M. *Current concepts and future directions in computer-aided diagnosis for CT colonography*. in *CARS 2002*, 2002.
6. Xu, C., D.L. Pham, and J. Prince. *Finding the brain cortex using fuzzy segmentation, isosurface, and deformable surface models*. in *the XVth Int. Conf. on Info. Proc. in Med. Img. (IPMI)*. 1997.
7. Kass, M., A. Witkin, and D. Terzopoulos, *Snakes: Active Contour Models*. International Journal of Computer Vision, 1988: p. 321-331.
8. Cohen, L.D., *On Active Contour Models and Ballons*. Computer Vision, Graphics, and Image Processing: Image Understanding, 1991. **53**(2, March 1991): p. 211-218.